Innovative aerosol hygroscopic growth study from Mie-Raman-Fluorescence lidar and Microwave Radiometer synergy

Robin Miri[1], Olivier Pujol[1], Qiaoyun Hu[1], Philippe Goloub[1], Igor Veselovskii[2,3], Thierry Podvin[1], Fabrice Ducos[1]

[1]Univ. Lille, CNRS, UMR 8518 – LOA – Laboratoire d'Optique Atmosphérique, Villeneuve d'Ascq 59650, France
[2]Prokhorov General Physics Institute of the Russian Academy of Sciences, Moscow, Russia
[3]Cimel Electronique, 172 rue de charonne 75011 Paris, France

Correspondence to: Robin Miri (robin.miri@univ-lille.fr)

Abstract. This study focuses on the characterization of aerosol hygroscopicity using remote sensing techniques. We employ a Mie-Raman-Fluorescence lidar (LILAS), developed at the ATOLL platform, Laboratoire d'Optique Atmosphérique, Lille, France, in combination with the RPG-HATPRO G5 microwave radiometer to enable continuous aerosol and water vapor monitoring. We identify hygroscopic growth cases when an aerosol layer exhibits an increase in both aerosol backscattering coefficient and relative humidity. By examining the fluorescence backscattering coefficient, which remains unaffected by the presence of water vapor, the potential temperature and the absolute humidity, we verify the homogeneity of the aerosol layer~~By examining the aerosol layer type, determined through a clustering method, the fluorescence backscattering coefficient, which remains unaffected by the presence of water vapor, and the absolute humidity, we verify the homogeneity of the aerosol layer~~. Consequently, the change in the backscattering coefficient is solely attributed to water uptake. The Hänel theory is employed to describe the evolution of the backscattering coefficient with relative humidity and introduces a hygroscopic coefficient, γ, which depends on the aerosol type. The particularity of this method revolves in the use of the fluorescence which is employed to take into account and correct the aerosol concentration variations in the layer. Case studies conducted on July 29 and March 9, 2021 examine respectively an urban and a smoke aerosol layer. For the urban case, γ is estimated as 0.47±0.03 at 532 nm; as for the smoke case, the estimation of γ is 0.5±0.3. These values align with those reported in the literature for urban and smoke particles. Our findings highlight the efficiency of the Mie-Raman-Fluorescence lidar and Microwave radiometer synergy in characterizing aerosol hygroscopicity. The results contribute to advance our understanding of atmospheric processes, aerosol-cloud interactions, and climate modeling.

Key words:

Aerosols, Hygroscopicity~~, Classification~~, Fluorescence Lidar, Microwave Radiometer

1 Introduction

Aerosols play a crucial role in our understanding of climate dynamics. Their impact on the radiation budget is classified into direct and semi-direct effects (Hansen et al., 1997; Thorsen et al., 2020), with additional contributions arising from aerosol-cloud interactions, commonly known as indirect effects. Certain aerosols can act as cloud condensation nuclei (CCN) or or ice nucleating particle (INP)ice nuclei (IN), altering cloud properties including albedo and lifetime (Twomey et al., 1967). These complex processes remain significant challenges in the interpretation of the Earth energy balance. To advance our comprehension of aerosol-cloud interactions is crucial for improving climate models and accurately accounting for their influence on the energy balance of our planet. A key process in the understanding of these interactions is hygroscopic growth, which consists in aerosol uptake of water vapor in high relative humidity (RH) conditions, resulting in changes in size and, in some cases, chemical composition (Hänel, 1976). Hygroscopic growth efficiency varies depending on the aerosol type, with hydrophobic aerosols like dust and hydrophilic aerosols like marine particles (Chen et al., 2019; Chen et al., 2020). This variability is linked to their potential as CCN and IN, highlighting the importance of understanding the hygroscopic properties of aerosols (G. McFiggans et al., 2006; U. Dusek et al., 2006).

Hygroscopic growth properties of aerosols can be effectively investigated using a range of instruments. Traditionally, humidified nephelometers and spectrometers have been widely used to study aerosol hygroscopicity (Covert et al., 1972; Burgos et al., 2019). However, active remote sensing systems tend appear more advantageous since the last decade as they allow to measure with high vertical and temporal resolution, without interfering with the observed system. Lidars, in particular, have gained prominence in remotely studying these properties (Feingold and Morley, 2003; Fernández et al., 2015; Granados-Muñoz et al., 2015; Zieger et al., 2015; Navas-Guzmán et al., 2019, Dawson et al., 2020; Düsing et al., 2021; Sicard et al. 2022…) and offer several advantages compared to other methods. In particular, lidars provide high vertical and temporal resolution, allowing for detailed analysis of aerosol characteristics. Moreover, lidars offer the unique capability of simultaneously measuring aerosol properties and water vapor mixing ratio using a single instrument. At the Laboratoire d'Optique Atmosphérique (LOA) in Lille, France, the ATOLL platform (ATmospheric Observations at LiLLe) features a Mie-Raman-Fluorescence lidar (Lille Lidar for Atmospheric Study, LILAS) employed in the frame of EARLINET/ACTRIS-FR. This multiwavelength lidar system measures elastic, depolarized and Raman signals, providing comprehensive information on aerosol properties. The elastic signal being the one coming from the elastic scattering of the laser light by atmospheric molecules and aerosols, the depolarized signal is the part of the elastic signal which either has kept the laser polarization or has been depolarized after the scattering, and finally the Raman signal refers to the inelastic scattering, or Raman scattering, by atmospheric molecules. Additionally, LILAS captures aerosol fluorescence signal at approximately 460 nm, which is triggered by the lidar UV wavelength at 355 nm. The fluorescence signal possesses distinctive characteristics that contribute to its utility in aerosol studies. Its intensity correlates with aerosol concentration and type, with biological aerosols like pollens or biomass burning exhibiting higher fluorescence, while pure dust or urban aerosols demonstrate lower fluorescence. Furthermore, the fluorescence signal at 460 nm does not arise from pure water, enabling the extraction of aerosol-specific

information without the influence of water vapor, which proves to be essential in studying aerosol hygroscopic growth (Veselovskii et al., 2020). In combination with an RPG-HATPRO G5 microwave radiometer, also part of the ATOLL platform, it is possible to monitor both aerosol characteristics and water vapor, allowing to study aerosol hygroscopicity.

The first part of this paper introduces the instruments, and outlines a novel method for the study of aerosol hygroscopic growth using LILAS measurements.~~The first part of this paper introduces the instruments, and outlines a novel method for an automatic aerosol classification, as well as for the study of aerosol hygroscopic growth using LILAS measurements~~. Following the instrument and method description, case studies are presented to demonstrate the efficiency and potential of the proposed approach. These case studies illustrate the practical implementation and feasibility of this innovative methodology, highlighting the added value brought by aerosol fluorescence measurement in offering valuable insights into the hygroscopic growth characteristics of these aerosols. Finally, the paper concludes with a summary of the findings and offers comments on the obtained results. The conclusions will also discuss the potential further advancements and applications of the developed method, emphasizing its importance in enhancing our understanding of hygroscopic growth phenomena and its broader implications for atmospheric research.

2 Instrumentation and methodology

2.1 Experimental setup and data treatment

All the measurements presented in this paper were performed at the ATOLL platform in Lille (50.611° N, 3.138° E). The first instrument used in this study is the lidar LILAS. Its ~~LILAS (Fig. 1)~~ emission component consists of a tripled Nd:YAG laser operating at a repetition rate of 20 Hz, with a pulse energy of 70mJ at 355nm. The lidar system is configured in the $3\beta + 2\alpha + 3\delta$ arrangement, meaning it measures the elastic backscatter coefficient at three wavelengths (355 nm, 532 nm and 1064 nm), it also measures the extinction at 355 nm and 532 nm, as well as the volume depolarization ratios for these wavelengths. This instrument also includes an additional channel dedicated to aerosol fluorescence detection featuring a dedicated interference filter centred at 466 nm with a width of 44 nm~~at 460 nm~~. For this study, the aerosol elastic backscatter coefficients (β) and the particulate depolarization ratio (PLDR) were computed at 532 nm from Mie-Raman observation (Ansmann et al., 1992) due to the low signal to noise ratio at this wavelength in comparison with the two others. Furthermore, the detection part of the lidar includes a channel specifically designed to measure the vibrational-rotational Raman scattering of water at 408 nm, allowing for the retrieval of water vapor mixing ratio profiles (Rao et al., 2002). The obtained profiles were acquired during night time only, and averaged over a period of 60 minutes. General details about the system can be found in Hu et al. (2018) and Veselovskii et al. (2020).

The proximity of the ATOLL platform to the airport prohibits the use of radiosounding. This poses a challenge for the inversion of water vapor using the LILAS lidar, as the computation of the instrumental constant requires a reference. Moreover, radiosoundings traditionally provide temperature profiles, which are crucial for calculating RH but are difficult to obtain otherwise.

The second instrument used in this study is the RPG-HATPRO G5 microwave radiometer developed by Radiometer Physics present at the ATOLL platform which provides integrated information like Integrated Water Vapor content (IWV) or Liquide Water Content (LWC), but also uses an integrated neural network model to retrieve atmospheric profiles of temperature, humidity, and liquid water. In situ sensors allow for ground level measurement of temperature, humidity and pressure. Finally, an infrared radiometer extension allows to detect cloud base height and ice clouds. Data are acquired at high temporal resolution (every 10 minutes) and profiles range from the ground to 10km (Louf et al., 2015).

This instrument has been considered to compensate for the lack of radiosounding measurement at the ATOLL platform for the calibration of the lidar water vapor measurement. Unfortunately, after considering using the radiometer humidity and temperature profiles for the lidar calibration, these ones turned out to be insufficiently accurate.

Consequently, temperature profiles from the ERA-5 reanalysis database were also collected, and the IWV measurement of the radiometer has been used to calibrate the lidar.

In order to compute the instrumental constant necessary for the lidar water vapor calibration, the radiometer IWV has been compared to the integral of absolute humidity (AH) between the ground and 6 km (above which humidity is negligible), derived from the lidar-measured water vapor mixing ratio and the ERA-5 temperature. Following the calibration procedure described in Foth et al. (2015), the calibration constant of the instrument is determined as the ratio between IWV and the integral value. The calibrated water vapor mixing ratio can be computed with:

In order to address these issues, temperature profiles from the ERA-5 reanalysis database were collected, and integrated water vapor content (IWV) measurements from the HATPRO microwave radiometer (Fig. 2), located on the ATOLL platform have been utilized. To calibrate LILAS, the IWV measurement has been compared to the integral of absolute humidity (AH) between the ground and 6 km, derived from the lidar-measured water vapor mixing ratio and the ERA-5 temperature. Following the calibration procedure described in Foth et al. (2015), the calibration constant of the instrument is determined as the ratio between IWV and the integral value. The calibrated water vapor mixing ratio can be computed with:

$$x_{H_2O}(h) = x'_{H_2O}(h) IWV \left[\int_0^{z_{max}} x'_{H_2O}(h) \frac{P(h)}{R_a T(h)} dh \right]^{-1} , \qquad (1)$$

where h is the height, $x_{H_2O}(h)$ and $x'_{H_2O}(h)$ the calibrated and not-calibrated water vapor mixing ratios respectively, z_{max} is equal to 6 km, P is the atmospheric pressure estimated with the hydrostatic approximation, R_a is the air perfect gas constant, T is the temperature all given in the International System of units (https://www.bipm.org/en/publications/si-brochure). The calibration has been exclusively conducted under clear sky conditions and taking into account the signal-to-noise ratio of the lidar's water vapor mixing ratio: between 5 and 6 km, if the signal to noise ratio is lower than 0.3, the calibration constant is not computed. Thise 0.3 threshold has been determined to ensure both data quality and a sufficient number of calibration constant computations. An interpolation has then been performed to estimate the calibration constants of cloudy and noisy situations.

125 Figure 1: Picture of LILAS (pi: Philippe Goloub, philippe.goloub@univ-lille.fr)

Figure 2: Picture of the HATPRO microwave radiometer (pi: Olivier Pujol, olivier.pujol@univ-lille.fr)

2.2 Classification method

The aerosol typing method developed in this paper is based on that presented by Veselovskii et al. (2022). This method mainly

130 relies on the PLDR at 532 nm, hereafter referred to as depolarization ratio for simplicity, and the aerosol fluorescence capacity (G_{Fluo}). G_{Fluo} is defined as the ratio of the fluorescence backscatter coefficient (β_{Fluo}) to the elastic backscatter coefficient at 532 nm (β_{532}). By analysing these two quantities, we can classify aerosols into four distinct types, as depicted in Figure 3.
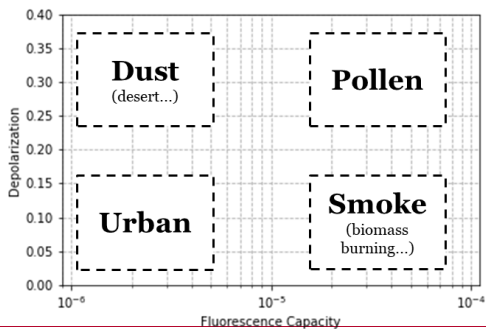
Figure 3: Schematic empirical aerosol typing repartition in function of the Depolarization (PLDR) & Fluorescence capacity (adapted from Veselovskii et al. 2022)

One of the primary limitations of this method lies in the treatment of hygroscopic growth scenarios. When hygroscopic growth takes place, the elastic backscatter coefficient increases, while the fluorescence backscatter coefficient is assumed to be unchanged (since water does not produce fluorescence at 460 nm (Veselovskii et al., 2020)), resulting in a reduction of the fluorescence capacity. Consequently, this situation can potentially lead to misclassification.

To address this challenge and account for the effect of hygroscopic growth, an automatic classification algorithm based on a Gaussian Mixture Model (GMM) has been developed, we have called it FLARE-GMM (Fluorescence Lidar based Aerosol REcognition with Gaussian Mixture Model). GMM is a clustering technique utilized to discern patterns within a dataset and recognize data clusters. It generates Gaussian probability functions, indicating the likelihood of belonging to each class, with the highest probability corresponding to the assigned class for each data point (Reynolds, 1992).

FLARE-GMM has been trained using nighttime lidar data collected during 2021 and 2022, as fluorescence and humidity can only be collected by night. For this automatic classification, both the fluorescence capacity and the depolarization ratio have been considered as features. Additionally, the algorithm takes RH into account to effectively handle cases involving hygroscopic growth. By incorporating these evolutions, FLARE-GMM becomes more robust and enables providing accurate aerosol typing even under varying hygroscopic conditions.

To train the model, the data selected for training purposes were restricted to altitudes above 1.5km. This decision has been taken in order to avoid most of the boundary layer, where significant mixing takes place, making it more challenging to identify distinct clusters. Furthermore, only instances where β_{532} fell within the range of $[1; 10]\ sr^{-1}.Mm^{-1}$ have been considered in order to exclude both cases with low aerosol concentrations which can be difficult to identify, as well as cloud-related data.

In order to determine the optimal number of clusters for classification, the silhouette coefficient (Aranganayagi et al., 2007), a classificator performance indicator, has been computed for different number of clusters (Rousseeuw et al., 1987). This coefficient, between -1 and 1, is an indicator that shows if a repartition fits the data, and is widely used to estimate the number

2.2~~3~~ Hygroscopic growth identification & study

In order to identify and analyze hygroscopic growth cases, a widely used method consists in searching for a homogeneous aerosol layer that spans either in time or altitude. When RH and elastic backscatter coefficient both increase, or decrease, it serves as a key indicator of hygroscopic growth. In such cases, the elastic backscatter coefficient evolution can be attributed only to hygroscopic growth. This approach enables to relate the elastic backscatter coefficient and RH, characterizing the hygroscopic properties of the considered aerosol particles.

The verification of the homogeneous nature of the considered aerosol layer is generally performed by investigating two key variables, absolute humidity and potential temperature, in order to identify any changes in the air mass. When these quantities show relative stability within the aerosol layer, it supports the hypothesis that the layer is homogeneous (Granados-Muñoz et al., 2015; Guzman et al., 2019; Sicard et al. 2022).

The focus of this paper rounds about the valuable insights provided by β_{fluo}. By assuming that hygroscopic growth does not impact aerosol fluorescence (Veselovskii et al., 2020), β_{fluo} becomes a reliable proxy for monitoring the concentration of dry material within the aerosol layer. Under the hypothesis of a constant aerosol mixture and chemical composition in the layer, normalizing β_{532} by β_{fluo} enables the study of hygroscopic growth properties, while also accounting for any possible changes in aerosol concentration within the layer.

Once the hygroscopic growth case has been identified, it becomes possible to examine the correlations between aerosol optical properties and RH. In this paper, particular attention has been given in the investigation of β_{532}. In order to explore this correlation efficiently, the Hänel parametrization has been used to express the changes in β_{532} as a function of RH. It introduces a parameter γ, known as the hygroscopic growth factor, which depends on the wavelength and the type of aerosol (Hänel, 1976). The Hänel parametrization is represented by:

$$\frac{\beta_{532}(\text{RH})}{\beta_{532}(\text{RH}_{\text{ref}})} = \left(\frac{100-\text{RH}}{100-\text{RH}_{\text{ref}}}\right)^{-\gamma}, \tag{2}$$

RH_{ref} being the reference relative humidity. We obtain an accurate estimation of the hygroscopic parameter γ, by fitting the variation of β_{532} with respect to RH to the function:

$$\beta_{532}(\text{RH}) = \beta_{532}(\text{RH}_{\text{min}})\frac{\beta_{fluo}(\text{RH})}{\beta_{fluo}(\text{RH}_{\text{min}})}\left(\frac{100-\text{RH}}{100-\text{RH}_{\text{min}}}\right)^{-\gamma}, \tag{3}$$

where RH_{min} represents the minimum relative humidity observed within the analysed aerosol layer.

Subsequently, the estimations of γ values can be compared to hygroscopic growth parameter estimations from previous studies, the type of the aerosol can be estimated from the optical properties, mainly its fluorescence capacity (the ratio between

the fluorescence and elastic backscatter coefficients) and PLDR (Veselovskii et al, 2022) as shown Figure 1. This comparative analysis offers valuable insights on how the hygroscopic growth of aerosols relates to their specific compositions and sources, contributing to a deeper understanding of aerosol behaviour in changing environmental conditions.
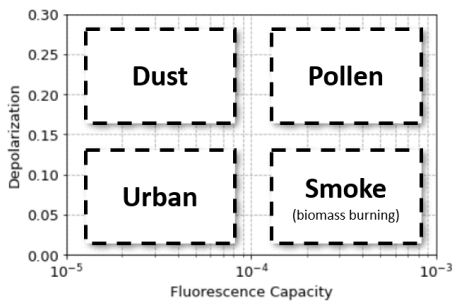
Figure 1: Schematic empirical aerosol typing repartition in function of the Depolarization (PLDR) & Fluorescence capacity (adapted from Veselovskii et al. 2022)

Subsequently, these estimated values can be compared to hygroscopic growth parameter estimations from previous studies, considering the aerosol types determined by FLARE-GMM. This comparative analysis offers valuable insights on how the hygroscopic growth of aerosols relates to their specific compositions and sources, contributing to a deeper understanding of aerosol behaviour in changing environmental conditions.

3 Results and discussions

3.1 Classification accuracy estimation

Assessing the accuracy of clustering models such as GMM can be challenging in the absence of definitive benchmarks. In this section, a first work has been performed to have an idea of FLARE-GMM performances to identify aerosol types from LILAS data.

Our initial approach involves scrutinizing the classification outcomes in instances where aerosol categories are unequivocally established. These situations mainly manifest during specific events of dust or smoke occurrences. The region of Lille frequently experiences such events, which are consistently documented and analysed by the LOA (Baars et al., 2019), and which origins can be checked from backward trajectories (Stein et al., 2015).

In order to illustrate this assessment approach, we first examine a dust event. In Lille, typically in March, substantial quantities of desert dust originating from the Sahara region are occasionally detected, largely attributable to Sirocco winds. These events materialized in both 2021 and 2022 and have been detected by LILAS. In Figure 4 are presented FLARE-GMM results for the

210 dust event cases of 2021 and 2022. These figures offer a visual depiction of the algorithm performance in such well defined aerosol situations.
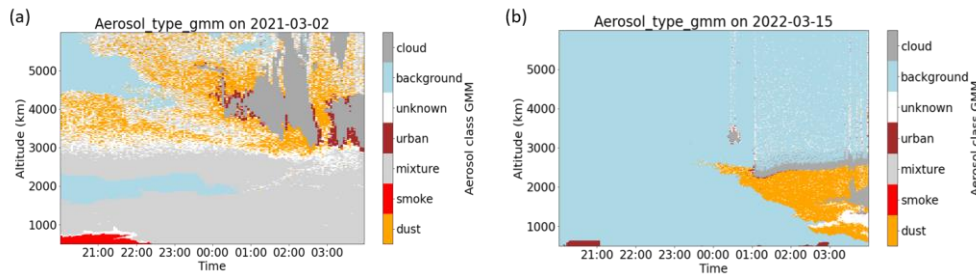
Figure 4: FLARE-GMM aerosol typing during the nights (a) from 2 to 3 March 2021 and (b) from 15 to 16 March 2022

Figure 4 presents the outcomes generated by the classification algorithm on lidar quicklooks. These quicklooks represent
215 unaveraged data with notable temporal and spatial resolutions. They are generated with the primary aim of enhancing our understanding of various atmospheric situations, at the expense of introducing greater measurement noise into the dataset. Among the results of the classification algorithm, thresholds on β_{532} have been applied to define the clear air and cloudy conditions, these thresholds have been arbitrarily fixed at 0.5 $Mm^{-1}.sr^{-1}$ bellow which the case is considered as background, or clear air, and 10 $Mm^{-1}.sr^{-1}$ above which the case is considered as cloud. The thresholds have been used because bellow
220 0.5 $Mm^{-1}.sr^{-1}$, the PLDR, being computed from a ratio, becomes extremely sensitive to noise, and over 10 $Mm^{-1}.sr^{-1}$, the situation is considered as cloudy and therefore much more difficult to analyze accurately. The unknown class is assigned to data points for which the GMM probability, denoting the likelihood of belonging to a specific class, falls below the 80% threshold.

Figure 4 visually validates the classification algorithm accuracy in identifying predominant dust layers. In the 2021 case, the
225 algorithm identifies a mixture of aerosols in the lower part of the layer, and a domination of dust in upper layer. In the 2022 case, the algorithm classifies it as a predominantly pure dust event. An interesting observation is made near the cloud region, where FLARE-GMM tends to associate the situation with urban aerosols. We acknowledge that this represents one of the algorithm limitations. Given that the classifier was not trained on cloudy scenarii, situations characterized by low depolarization and limited fluorescence capacity tend to be erroneously classified as urban aerosols in the vicinity of clouds.
230 This issue is however specific to the quicklooks and is a consequence of the high temporal and spatial measurement resolution. Regarding smoke events, a significant occurrence was the fires near Bordeaux in July 2022. The smoke aerosols originating from this region were observable at ATOLL during the period approximately spanning from July 17 to July 20. Figure 5

illustrates the outcomes of FLARE GMM for this particular scenario and demonstrates that in this instance, the layer is accurately categorized as a smoke layer, highlighting the algorithm capability to detect such events.

235
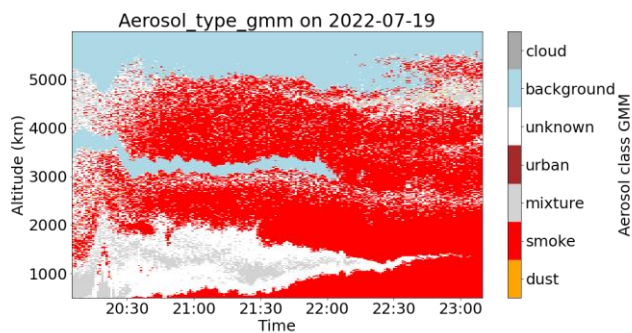
Figure 5: FLARE-GMM estimation of aerosol class during the night on 19 July 2022

Figure 4 and Figure 5 illustrate the algorithm ability to discriminate extreme events during substantial pure dust and smoke events. These specific examples provide compelling evidence that the algorithm accurately identifies instances of pure smoke and dust, clearly discriminating them from other aerosol types. This, in turn, enhances the overall confidence in the algorithm
240 results.

An alternative method employed to assess FLARE GMM accuracy consists in comparing it to a relative reference. In this capacity, NATALI (Neural Network Aerosol Typing Algorithm Based on Lidar Data), another automated classifier relying on lidar data, has been used. By juxtaposing the outcomes obtained from NATALI, whose accuracy is estimated at approximately 70% (Nicolae et al., 2018, Papagiannopoulos et al., 2018), with FLARE GMM outcomes, it becomes feasible to estimate the
245 relative accuracy of the latter. This method is however imperfect because the comparison does not yield absolute accuracy. Instead, it offers a rough approximation of the classifier performance. The comparative analysis has been conducted on 38 profiles from the year 2022. The findings are presented in a confusion matrix (Fig. 6).
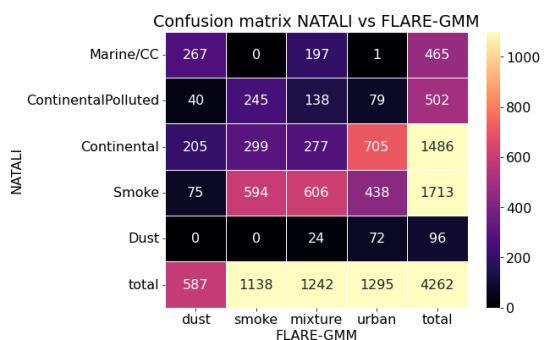
~~Figure 6 shows the confusions matrix between the results from FLARE-GMM and NATALI on 38 profiles of 2022. The confusions matrix shows the correspondence between the number of identified cases of each class, these matrixes are regularly used to assess the performance of a classifier in machine learning, by comparing the model results to a reference. In this case, the confusion matrix illustrates disparities in the outcomes between NATALI and FLARE-GMM in various aspects. On one hand, concerning the classification of dust, it appears that the dust cases identified by FLARE-GMM are often categorized as Marine/CC by NATALI. This outcome may appear unexpected, given the ATOLL's inherent characteristics, which typically result in a very low presence of marine aerosols. These differences could be explained by two aspects. First, NATALI bases its classification on the lidar ratio (LR) and the Angstrom exponent, both parameters highly susceptible to measurement uncertainties which might introduce errors in aerosol typing. Moreover, the dataset employed to train NATALI consists of simulated data, which might introduce bias in classifying data obtained from the LILAS system, generated from the specificities of both the instrument and Lille atmospheric conditions. In contrast, FLARE-GMM is directly trained on LILAS data, enhancing its performance.~~

~~On the other hand, when examining urban and smoke cases, it becomes obvious that the results from the two models diverge, with numerous cases identified by NATALI as smoke, classified as urban by FLARE-GMM. An explanation is that FLARE-GMM could present a bias towards urban cases, possibly due to hygroscopic growth. This growth diminishes the smoke fluorescence capacity, leading to misclassifications as urban aerosols. However, it is worth noting that this issue should have been addressed, given that RH is integrated as a feature in the model. Therefore, a situation with high RH and relatively low fluorescence capacity can still be correctly identified as a smoke case. The explanation could also stem from the assumptions made in the former paragraph.~~

~~In conclusion, while drawing precise quantitative conclusions about FLARE-GMM accuracy may be challenging, the comparison with NATALI provides encouraging results, with a substantial agreement between the two models (approximately~~

3.2 Hygroscopic growth methodology study

275 In order to experiment the potential of the hygroscopic growth study approach, this method has been tested on two potential hygroscopic growth cases, the first one occurring during 29 July 2021, averaged from 22:00 to 23:00 UTC, and the second during 9 March 2021, averaged from 21:00 to 22:00 UTC.
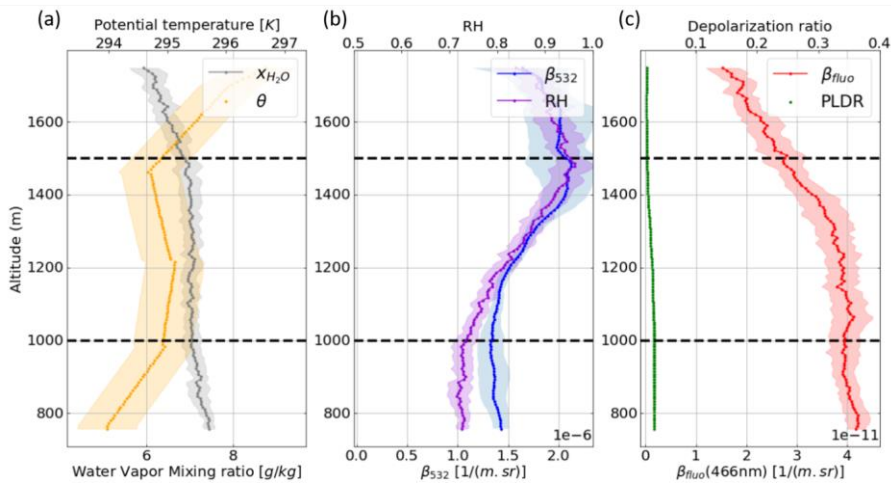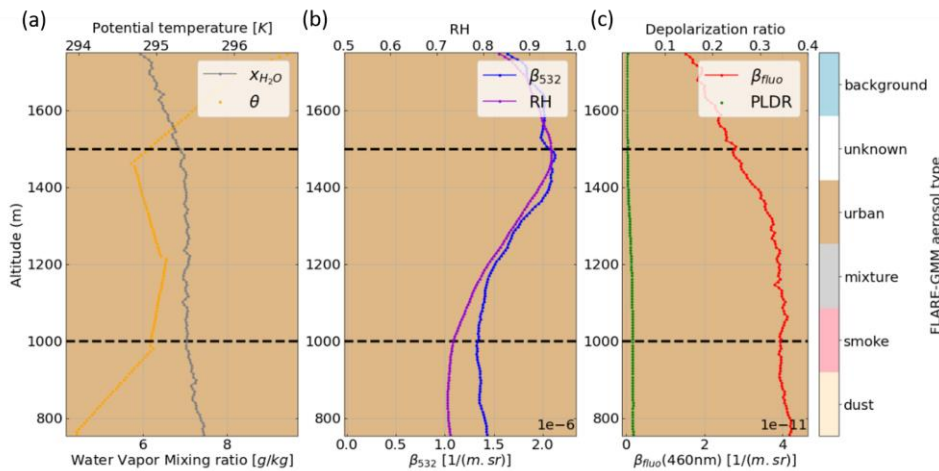
Figure 2: Profile of retrieved optical properties in function of altitude above ground level (a) water vapor mixing ratio [g/kg] and potential temperature [K], (b) elastic backscatter coefficient at 532 nm [1/m.sr] and RH, (c) fluorescence backscatter coefficient at 466 nm [1/m.sr] and particular linear depolarization ratio at 532 nm, on 29 July 2021 at 22:00 UTC, the black dashed lines identify the area where hygroscopic growth is expected to occur

Figure 2 shows the profiles of the different measurements on the case study of 29 July 2021. In this particular scenario, both the water vapor mixing ratio and potential temperature exhibit relative stability, which are the two criteria commonly used to assess that the considered aerosol layer is homogeneous (Granados-Muñoz et al., 2015; Guzman et al., 2019; Sicard et al., 2022). Even though the potential temperature is derived from model estimations rather than direct measurements, this still provides a strong indication of the aerosol layer homogeneity. Moreover, the β_{fluo} does not show strong variations within the defined region (the standard deviation of β_{fluo} in the considered layer is about 10% of the average), further supporting this conclusion. ~~remains highly stable within the defined region, as does the class determined by FLARE-GMM, further supporting this conclusion.~~

Conversely, there is an increase in both β_{532} and RH, suggesting a potential case of hygroscopic growth. RH rises from 74% to 96% which is a significant growth and strongly support the hypothesis that hygroscopic growth occurs. Lastly, the PLDR slightly decreases, but given its already low value, further decrease due to hygroscopic growth is not anticipated.

Finally, it is possible to estimate the aerosol type of the considered layer by looking at its optical properties. Figure 3 shows the scatter plot of the PLDR at 532 nm and the fluorescence capacity which is here the ratio between β_{fluo} and β_{532}. The considered aerosol layer exhibits low PLDR as well as low fluorescence capacity, characteristics that allow it to be identified as an urban aerosol layer.

~~A limitation to consider in this situation is that the studied layer is below 1500 m. This is due to the lack of nice hygroscopic growth cases in high altitudes in the dataset used in this study. As mentioned, FLARE-GMM has not been trained on data bellow this threshold, so it could potentially lead to a drop of performance. However, since the optical characteristics of an aerosol type are the same bellow this threshold, the classification performance is not expected to drop. The outcomes of the fitting process to the Hänel parametrization are displayed in Figure 8.~~
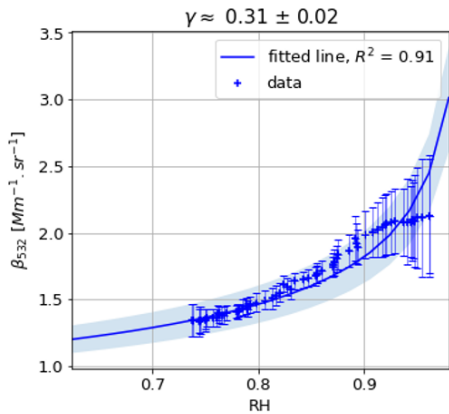
Figure 4: Evolution of the elastic backscatter coefficient at 532 nm in function of RH on 29 July 2021 at 22:00 UTC between 1000 m and 1500 m above ground level, and results of the fit on the Hänel parametrization

~~Figure 8: Evolution of β_{532} in function of RH on 29 July 2021 at 10 pm between 1000 m and 1500 m, and results of the fit on the Hänel parametrization~~

Figure ~~8~~4 presents the outcomes of the fitting process for the relationship between β_{532} and RH using the Hänel parametrization. These results indicate a good fit to the Hänel parametrization in this particular case, as evidenced by the

determination coefficient being close to 1 ($R^2 = 0.91$). However, the estimated value of γ, which is expected to fall between 0.3 and 0.5 for a case of urban particles (Guzman et al., 2019), is equal to 0.3 in this instance, which is very close to the lower limit for this type of aerosols. It also comes along with a slight divergence between the fit and the data, specially at high RH. Several factors may contribute to the deterioration of the results and explain the low value of γ. First, it is possible that in this

325 case, there is merely no significant hygroscopic growth occurring for this particular type of aerosol within the observed range of RH. However, given the substantial RH variation, starting at 74% and reaching up to 96%, this hypothesis becomes less plausible.

Second, it is possible that the main assumption on which lies this parametrization,of the study, i.e. constant aerosol concentration within the observed layer, may not hold true. Even with stable potential temperature and water vapor mixing

330 ratio, there is a possibility that aerosol concentration varies within the designated area, especially considering that potential temperature is derived from models and not directly measured. This variation could potentially account for the low estimation of the hygroscopic growth factor.

In order to investigate this, we can assume that aerosol mixing remains constant within the study area, and that β_{fluo} varies solely with changes in aerosol concentration. Doing so, it becomes possible to normalize β_{532} based on variations in aerosol

335 concentration according to:

$$\overline{\beta_{532}}(\text{RH}) = \beta_{532}(\text{RH})\frac{\beta_{fluo}(\text{RH}_{min})}{\beta_{fluo}(\text{RH})}, \tag{4}$$

Here, $\overline{\beta_{532}}(\text{RH})$ is the normalized elastic backscatter coefficient and $\beta_{fluo}(\text{RH}_{min})$ is β_{fluo} at the minimum value of RH in the studied area.

It is now possible to apply the Hänel parametrization on $\overline{\beta_{532}}$ instead of β_{532} to take into account aerosol concentration

340 variations within the layer, and assess whether this normalization yields improved results. The relationship between $\overline{\beta_{532}}$ and RH, along with its fit to the Hänel parametrization is presented in Figure 9.
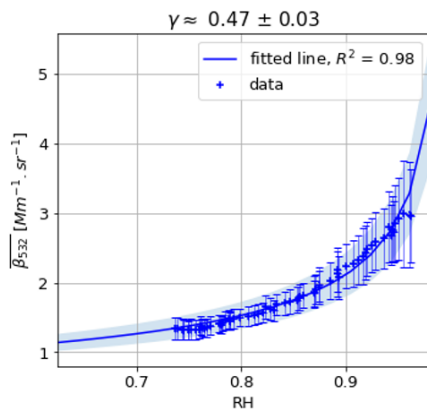
Figure 5: Evolution of the normalized elastic backscatter coefficient at 532 nm (normalized with fluorescence backscatter coefficient) in function of RH on 29 July 2021 at 22:00 UTC between 1000 m and 1500 m above ground level, and results of the fit on the Hänel parametrization

~~**Figure 9: Evolution of $\overline{\beta_{532}}$ in function of RH on 29 July 2021 at 10 pm between 1000 m and 1500 m, and results of the fit on the Hänel parametrization**~~

The relationship between $\overline{\beta_{532}}$ and RH, along with its fit to the Hänel parametrization presented in Figure 5 demonstrate a significantly improved fit to the Hänel parametrization~~The results presented in Figure 9 demonstrate a significantly improved fit to the Hänel parametrization~~, with a notably higher determination coefficient ($R^2 = 0.98$ instead of 0.91). Furthermore, the estimation of γ is found to be equal to 0.47 ± 0.03, falling precisely within the range of estimations conducted at 532nm by previous studies (Guzman et al. 2019, Sicard et al. 2022). These findings support the hypothesis that aerosol concentration varies within the aerosol layer, and that such fluctuations are traceable through β_{fluo}, corroborating the efficiency of the presented approach for investigating hygroscopic growth phenomena.

Another case study can be presented to further support the validity of this approach. It is the case occurring on on 9 March 2021 averaged between 21:00 UTC and 22:00 UTC.
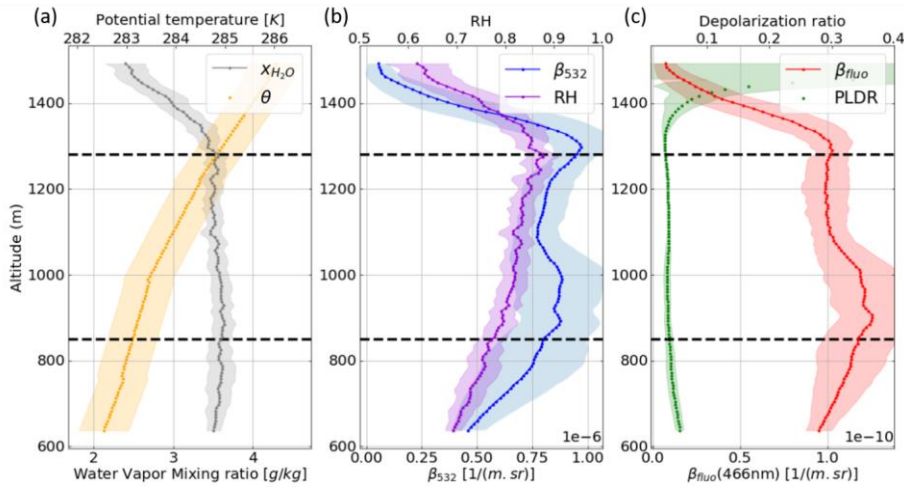
Figure 6: Profile of retrieved optical properties in function of altitude above ground level (a) water vapor mixing ratio [g/kg] and potential temperature [K], (b) elastic backscatter coefficient at 532 nm [1/m.sr] and relative humidity, (c) fluorescence backscatter coefficient at 466 nm [1/m.sr] and particular linear depolarization ratio at 532 nm, on 9 March 2021 at 21:00 UTC, the black dashed lines identify the area where hygroscopic growth is expected to occur
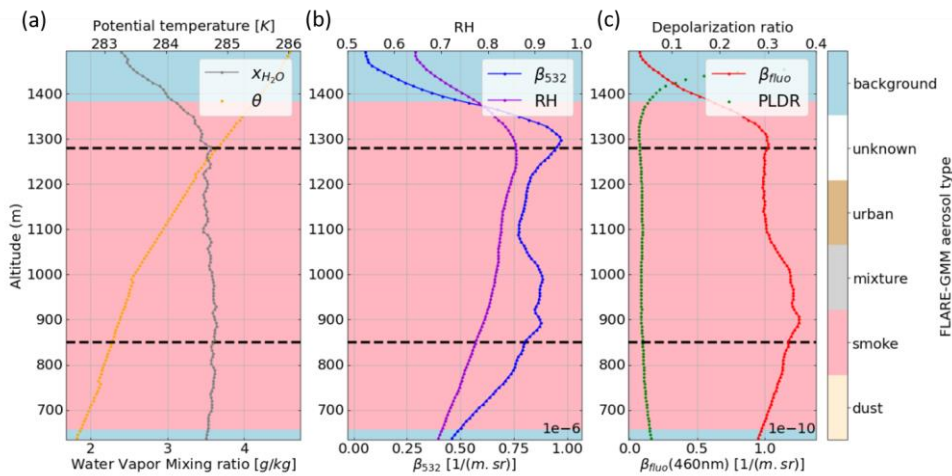
Figure 6 shows the profiles of the different measurements on the case study of 9 March 2021. In this situation, both the water vapor mixing ratio and the potential temperature are relatively stable in the layer (potential temperature variations remain under 2 K, and the water vapor mixing ratio variations remain under 1 g/kg), indicating a good mixing in the considered layer. An increase in both RH and β_{532} can also be noticed. On the other hand, there are fluctuations of is a small variation of β_{fluo}, mostly in the lower part of the layer, and the PLDR remains stable, but once again, given its already low value, it is not expected to decrease with hygroscopic growth. These elements together indicate that a hygroscopic growth scenario is most likely to occur in this layer.

The aerosol type can be investigating once again by looking at the fluorescence capacity and the PLDR. Both are represented Figure 7 and show characteristics indicating that the aerosol layer comes from biomass burning smoke with low PLDR and strong fluorescence. Something worth noticing however is the low value of the fluorescence capacity. Indeed, the fluorescence capacity is the ratio between fluorescence backscatter coefficient and elastic backscatter coefficient. While the first one is expected to remain stable with hygroscopic growth, the second increases in high humidity condition, consequently decreasing the fluorescence capacity and potentially leading to misclassification as indicated in Veselovskii et al., 2020. In this case however, it is still possible to identify the biomass burning smoke aerosol layer.

The evolution of both β_{532} and $\overline{\beta_{532}}$ with RH can be fitted using the Hänel parametrization (Figure 11).
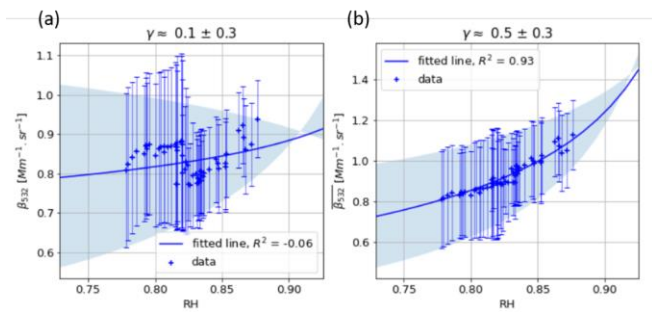
Figure 7: Evolution of the elastic backscatter coefficient at 532 nm (a) without normalization and (b) with normalization with the fluorescence backscatter coefficient, in function of RH on 9 March 2021 at 21:00 UTC between 850 m and 1280 m above ground level, and results of the fit on the Hänel parametrization

The results of the fit to the Hänel parametrization on both β_{532} and $\overline{\beta_{532}}$ indicate a significant improvement brought by the normalization with the fluorescence. Without this process, the fit to the Hänel parametrization is extremely poor, with $R^2 = -0.06$. Furthermore, the estimation of the hygroscopic growth parameter is much lower than expected ($\gamma = 0.1\cancel{1} \pm 0.3\cancel{28}$) while the value is expected to fall around 0.5 at 532 nm for smoke aerosols according to Gomez et al. (2018). On the other hand, by using the information given by the fluorescence to normalize the elastic backscatter coefficient, it is possible to obtain a much better fit to the Hänel parametrization, with $R^2 = 0.93$ and a better estimation of the hygroscopic growth parameter, with $\gamma = 0.5 \pm 0.3$ falling in the expected range for smoke aerosols. These findings suggest that it is indeed possible to use β_{fluo} to correct the variation of aerosol concentration within the aerosol layer to study hygroscopic growth. The only drawback of this case lays in its high uncertainty.

Explanation for this high uncertainty could be instrumental noise, or the span of RH covered being narrower than the first presented case (RH varying from 77.8% to 87.6%), or even the atmospheric variability being more important in this situation. Nevertheless, the point demonstrated in this analysis relies in the utility of the fluorescence correction for the hygroscopic factor estimation which is well emphasized here.

The influence of a shift in RH on γ has also been examined. For the case of 9 March 2021, when RH is decreased by 0.1$\cancel{10\%}$, the corresponding γ value becomes 0.82, while an increase of 0.1$\cancel{10\%}$ in RH results in a γ value of 0.23. The estimation of RH is based on both measurement from LILAS but also on ERA-5 reanalysis data, which heavily relies on computational models. While this estimation provides valuable insights, it inherently introduces a level of uncertainty on the results. It is anticipated that the uncertainty associated with this estimation falls within the range of 10%. The estimation of γ and the conclusions draw

from this estimation should then be considered with caution. Future studies might focus on refining the methods used for RH estimation, aiming at minimizing this inherent uncertainty and enhancing the accuracy of these findings. However, even if a shift in RH introduces high variability in γ, the determination coefficient R^2 remains almost unchanged ($R^2 = 0.92$ when RH is decreased by 0.1~~10%~~ and $R^2 = 0.91$ for a 0.1~~10%~~ increase) meaning that the conclusion drawn on the use of the fluorescence correction are still valid in spite of the uncertainty on RH.

4. Conclusion

In this article, we have examined the possibility of using LILAS data for aerosol typing and aerosol hygroscopic growth studies. The calibration of LILAS's water vapor channel has been addressed using thermodynamic data from the RPG-HATPRO microwave radiometer and temperature data from ERA-5 reanalysis. A new approach to analyse aerosol hygroscopicity, relying on the fluorescence profiles measured by LILAS has been developed and tested on two situations.

~~A novel classification, FLARE-GMM typing has been developed as well as a new approach to analyse aerosol hygroscopicity, both relying on the fluorescence profiles measured by LILAS.~~

~~The classification, FLARE-GMM is a Gaussian Mixture Model trained on LILAS profiles collected during 2021 and 2022. This model incorporates fluorescence capacity, particular linear depolarization ratios, and RH as features. The outcome of FLARE-GMM enables the categorization of aerosol layers into four distinct classes: dust, smoke, urban, or a mixture thereof. FLARE-GMM's performance has been assessed in specific aerosol events, such as the transport of Saharan dust or smoke plumes from southern France. In these instances, the model demonstrates accurate aerosol layer classifications.~~

~~FLARE-GMM results have also been compared to another classifier, NATALI, also relying on lidar data. Although the comparison presents analytical challenges and raises questions regarding the treatment of dust events and the confusion between smoke and urban aerosols. It also yields promising results, providing valuable insights into the FLARE-GMM accuracy and potential avenues for further research in aerosol characterization. Further studies will explore the enhancement of this method since features will be be added such as multiwavelength depolarization ratios, or more complex features such as the lidar ratio, or the Angstrom exponent.~~

~~Further work will enlarge the classification to aerosol layers located above 6 km, despite the limited availability of humidity data, or during daytime conditions when both humidity and fluorescence measurements are challenging.~~

~~Regarding the hygroscopic growth study, T~~the unique feature of the method presented in this article hinges on its use of the fluorescence backscatter coefficient. This coefficient serves as a weighting factor in tracking the evolution of aerosol concentration within the aerosol layer. Consequently, it leads to a significantly improved representation of the hygroscopic state evolution of the aerosols, thereby enhancing the characterization of the Hänel hygroscopic coefficient, γ. To validate this approach, evaluations were performed on two cases from July and March 2021, yielding promising results and highlighting the value brought by the fluorescence backscatter coefficient measurement with the lidar. With, in the first case, an estimation of γ of 0.47 ± 0.03 with the fluorescence correction, falling in the expected range of hygroscopic growth parameter of and

urban aerosol layer at 532 nm. In the second case, the estimation of γ is of 0.5 ± 0.3 which, despite higher uncertainty, is in the expected values for smoke particles at 532 nm and most importantly, is a great improvement compared to the estimation carried on without the fluorescence correction.

In order to further increase the accuracy of our results, radiosoundings could be used in order to better estimate RH, a variable that significantly influences γ estimation. Based on the presented approach, values of γ can be calculated for various types of aerosols, and the assessment of the relationship between γ and aerosol optical properties like PLDR or fluorescence capacity can be considered. However, a current limitation of the present work arises in the identification of hygroscopic growth cases which is made manually. Future efforts could focus on automatically identifying hygroscopic growth cases using lidar measurements, simplifying the study of γ dependency with aerosol parameters on a large number of situations (Gysel et al., 2007). These relationships are expected to provide valuable insights for modelling interactions between aerosols and water vapor, serving as an initial step in studying aerosol-cloud interactions (Dusek et al., 2006, Petters et al., 2007).

However, a current limitation of the present work arises in the identification of hygroscopic growth cases which is made manually. Future efforts could focus on automatically identifying hygroscopic growth cases using lidar measurements, simplifying the study of γ dependency with aerosol parameters on a large number of situations (Gysel et al., 2007). In this perspective, an automatic classification method is also currently being developed using clustering approach in order to automatically classify aerosol layers based on their optical properties as well as thermodynamic parameters accounting for humidity impact on the fluorescence capacity as illustrated in the analysis of Figure 7.

Furthermore, both the classification and the hygroscopic growth study will be adapted and improved for the LIFE lidar (Laser Induced Fluorescence Explorer), anticipated to be operational by 2024. This upcoming lidar system is set to have more power and include additional fluorescence channels, thereby increasing the amount of information available, which will significantly enhance the performance of the classification and provide greater precision in aerosol typing.

Code and data availability

Data and code will be available upon the request

Competing interests

The contact author has declared that none of the authors has any competing interests.

Acknowledgements

We acknowledge CaPPA project funded by the ANR through the PIA under contract ANR-11-LABX-0005-01. The authors thank the Région Hauts-de-France, the Ministère de l'Enseignement Supérieur et de la Recherche and the European Fund for

Regional Economic Development for their financial support to the CPER CLIMIBIO and ECRIN programs. The contribution from Q. Hu was supported by Agence Nationale de Recherche ANR (ANR-21-ESRE-0013) through the OBS4CLIM project. ChatGPT has been employed for the drafting purposes in this document.

470 **References**

Aranganayagi, S., and K. Thangavel. 2007. "Clustering Categorical Data Using Silhouette Coefficient as a Relocating Measure." In *International Conference on Computational Intelligence and Multimedia Applications (ICCIMA 2007)*, 13–17. Sivakasi, Tamil Nadu, India: IEEE. https://doi.org/10.1109/ICCIMA.2007.328.

475 Burgos, M.A., Andrews, E., Titos, G. et al. A global view on the effect of water uptake on aerosol particle light scattering. Sci Data 6, 157 (2019). https://doi.org/10.1038/s41597-019-0158-7

Baars, H., Ansmann, A., Ohneiser, K., Haarig, M., Engelmann, R., Althausen, D., Hanssen, I., Gausa, M., Pietruczuk, A., Szkop, A., Stachlewska, I. S., Wang, D., Reichardt, J., Skupin, A., Mattis, I., Trickl, T., Vogelmann, H., Navas-Guzmán, F., Haefele, A., Acheson, K., Ruth, A. A., Tatarov, B., Müller, D., Hu, Q., Podvin, T., Goloub, P., Veselovskii, I., Pietras, C., Haeffelin, M., Fréville, P., Sicard, M., Comerón, A., Fernández García, A. J., Molero Menéndez, F., Córdoba-Jabonero, C., Guerrero Rascado, J. L., Alados-Arboledas, L., Bortoli, D., Costa, M. J., Dionisi, D., Liberti, G. L., Wang, X., Sannino, A., Papagiannopoulos, N., Boselli, A., Mona, L., D'Amico, G., Romano, S., Perrone, M. R., Belegante, L., Nicolae, D., Grigorov, I., Gialitaki, A., Amiridis, V., Soupiona, O., Papayannis, A., Mamouri, R. E., Nisantzi, A., Heese, B., Hofer, J., Schechner, Y. Y., Wandinger, U., and Pappalardo, G.: The unprecedented 2017–2018 stratospheric smoke event: decay phase and aerosol properties observed with the EARLINET, Atmos. Chem. Phys., 19, 15183–15198, https://doi.org/10.5194/acp-19-15183-2019, 2019.

Chen, Jun, Zhanqing Li, Min Lv, Yuying Wang, Wei Wang, Yingjie Zhang, Haofei Wang, Xing Yan, Yele Sun, and Maureen Cribb. 2019. "Aerosol Hygroscopic Growth, Contributing Factors, and Impact on Haze Events in a Severely Polluted Region in Northern China." *Atmospheric Chemistry and Physics* 19 (2): 1327–42. https://doi.org/10.5194/acp-19-1327-2019.

Chen, Lanxiadi, Chao Peng, Athanasios Nenes, Wenjun Gu, Hanjing Fu, Xing Jian, Huanhuan Zhang, et al. 2020. "On Mineral Dust Aerosol Hygroscopicity." Preprint. Aerosols/Laboratory Studies/Troposphere/Chemistry (chemical composition and reactions). https://doi.org/10.5194/acp-2020-442.

495 Covert, D. S., R. J. Charlson, and N. C. Ahlquist, 1972: A Study of the Relationship of Chemical Composition and Humidity to Light Scattering by Aerosols. *J. Appl. Meteor. Climatol.*, **11**, 968–976, https://doi.org/10.1175/1520-0450(1972)011<0968:ASOTRO>2.0.CO;2.

Dawson, K. W., R. A. Ferrare, R. H. Moore, M. B. Clayton, T. J. Thorsen, and E. W. Eloranta. 2020. "Ambient Aerosol Hygroscopic Growth From Combined Raman Lidar and HSRL." *Journal of Geophysical Research: Atmospheres* 125 (7): e2019JD031708. https://doi.org/10.1029/2019JD031708.

Dusek, U., G. P. Frank, L. Hildebrandt, J. Curtius, J. Schneider, S. Walter, D. Chand, et al. 2006. "Size Matters More Than Chemistry for Cloud-Nucleating Ability of Aerosol Particles." *Science* 312 (5778): 1375–78. https://doi.org/10.1126/science.1125261.

Düsing, S., Ansmann, A., Baars, H., Corbin, J. C., Denjean, C., Gysel-Beer, M., Müller, T., Poulain, L., Siebert, H., Spindler, G., Tuch, T., Wehner, B., and Wiedensohler, A.: Measurement report: Comparison of airborne, in situ measured, lidar-based, and modeled aerosol optical properties in the central European background – identifying sources of deviations, Atmos. Chem. Phys., 21, 16745–16773, https://doi.org/10.5194/acp-21-16745-2021, 2021.

Feingold, Graham, and Bruce Morley. 2003. "Aerosol Hygroscopic Properties as Measured by Lidar and Comparison with in Situ Measurements." *Journal of Geophysical Research: Atmospheres* 108 (D11): 2002JD002842. https://doi.org/10.1029/2002JD002842.

Fernández, A.J., A. Apituley, I. Veselovskii, A. Suvorina, J. Henzing, M. Pujadas, and B. Artíñano. 2015. "Study of Aerosol Hygroscopic Events over the Cabauw Experimental Site for Atmospheric Research (CESAR) Using the Multi-Wavelength Raman Lidar Caeli." *Atmospheric Environment* 120 (November): 484–98. https://doi.org/10.1016/j.atmosenv.2015.08.079.

Foth, A., H. Baars, P. Di Girolamo, and B. Pospichal. 2015. "Water Vapour Profiles from Raman Lidar Automatically Calibrated by Microwave Radiometer Data during HOPE." *Atmospheric Chemistry and Physics* 15 (14): 7753–63. https://doi.org/10.5194/acp-15-7753-2015.

Gomez, S. L., C. M. Carrico, C. Allen, J. Lam, S. Dabli, A. P. Sullivan, A. C. Aiken, et al. 2018. "Southwestern U.S. Biomass Burning Smoke Hygroscopicity: The Role of Plant Phenology, Chemical Composition, and Combustion Properties." *Journal of Geophysical Research: Atmospheres* 123 (10): 5416–32. https://doi.org/10.1029/2017JD028162.

Gysel, M., J. Crosier, D. O. Topping, J. D. Whitehead, K. N. Bower, M. J. Cubison, P. I. Williams, M. J. Flynn, G. B. McFiggans, and H. Coe. 2007. "Closure Study between Chemical Composition and Hygroscopic Growth of Aerosol Particles during TORCH2." *Atmospheric Chemistry and Physics* 7 (24): 6131–44. https://doi.org/10.5194/acp-7-6131-2007.

Hänel, Gottfried. 1976. "The Properties of Atmospheric Aerosol Particles as Functions of the Relative Humidity at Thermodynamic Equilibrium with the Surrounding Moist Air." In *Advances in Geophysics*, 19:73–188. Elsevier. https://doi.org/10.1016/S0065-2687(08)60142-9.

Hansen, J., M. Sato, and R. Ruedy. 1997. "Radiative Forcing and Climate Response." *Journal of Geophysical Research: Atmospheres* 102 (D6): 6831–64. https://doi.org/10.1029/96JD03436.

Hu, Qiaoyun. 2018. "Advanced aerosol characterization using sun/sky photometer and multi-wavelength Mie-Raman lidar measurements."

Louf, V., Pujol, O., Sauvageot, H., Riédi, J., 2015. Seasonal and diurnal water vapour distribution in the sahelian area from microwave radiometric profiling observations. Quarterly Journal of the Royal Meteorological Society 141, 2643–2653. doi:10.1002/qj.2550

Navas-Guzmán, Francisco, Giovanni Martucci, Martine Collaud Coen, María José Granados-Muñoz, Maxime Hervo, Michael Sicard, and Alexander Haefele. 2019. "Characterization of Aerosol Hygroscopicity Using Raman Lidar Measurements at the EARLINET Station of Payerne." *Atmospheric Chemistry and Physics* 19 (18): 11651–68. https://doi.org/10.5194/acp-19-11651-2019.

Petters, M. D. and Kreidenweis, S. M.: A single parameter representation of hygroscopic growth and cloud condensation nucleus activity, Atmos. Chem. Phys., 7, 1961–1971, https://doi.org/10.5194/acp-7-1961-2007, 2007.

Nicolae, Doina, Jeni Vasilescu, Camelia Talianu, Ioannis Binietoglou, Victor Nicolae, Simona Andrei, and Bogdan Antonescu. 2018. "A Neural Network Aerosol-Typing Algorithm Based on Lidar Data." *Atmospheric Chemistry and Physics* 18 (19): 14511–37. https://doi.org/10.5194/acp-18-14511-2018.

Papagiannopoulos, Nikolaos, Lucia Mona, Aldo Amodeo, Giuseppe D'Amico, Pilar Gumà Claramunt, Gelsomina Pappalardo, Lucas Alados-Arboledas, et al. 2018. "An Automatic Observation-Based Aerosol Typing Method for EARLINET." *Atmospheric Chemistry and Physics* 18 (21): 15879–901. https://doi.org/10.5194/acp-18-15879-2018.

Petters, M. D. and Kreidenweis, S. M.: A single parameter representation of hygroscopic growth and cloud condensation nucleus activity, Atmos. Chem. Phys., 7, 1961–1971, https://doi.org/10.5194/acp-7-1961-2007, 2007.

Rousseeuw, Peter J. 1987. "Silhouettes: A Graphical Aid to the Interpretation and Validation of Cluster Analysis." *Journal of Computational and Applied Mathematics* 20 (November): 53–65. https://doi.org/10.1016/0377-0427(87)90125-7.

Sicard, M., Fortunato dos Santos Oliveira, D. C., Muñoz-Porcar, C., Gil-Díaz, C., Comerón, A., Rodríguez-Gómez, A., and Dios Otín, F.: Measurement report: Spectral and statistical analysis of aerosol hygroscopic growth from multi-wavelength lidar measurements in Barcelona, Spain, Atmos. Chem. Phys., 22, 7681–7697, https://doi.org/10.5194/acp-22-7681-2022, 2022.

Thorsen, Tyler J., Richard A. Ferrare, Seiji Kato, and David M. Winker. 2020. "Aerosol Direct Radiative Effect Sensitivity Analysis." Journal of Climate 33 (14): 6119–39. https://doi.org/10.1175/JCLI-D-19-0669.1.

Twomey, S., and J. Warner, 1967: Comparison of Measurements of Cloud Droplets and Cloud Nuclei. J. Atmos. Sci., 24, 702–703, https://doi.org/10.1175/1520-0469(1967)024<0702:COMOCD>2.0.CO;2.

Veselovskii, Igor, Qiaoyun Hu, Albert Ansmann, Philippe Goloub, Thierry Podvin, and Mikhail Korenskiy. 2021. "Fluorescence Lidar Observations of Wildfire Smoke inside Cirrus: A Contribution to Smoke-Cirrus – Interaction

565   Research." Preprint. Aerosols/Remote Sensing/Troposphere/Physics (physical properties and processes). https://doi.org/10.5194/acp-2021-1017.

Veselovskii, Igor, Qiaoyun Hu, Philippe Goloub, Thierry Podvin, Boris Barchunov, and Mikhail Korenskii. 2022a. "Combining of Mie-Raman and Fluorescence Observations: A Step Forward in Aerosol Classification with Lidar Technology." Preprint. Aerosols/Remote Sensing/Data Processing and Information Retrieval. https://doi.org/10.5194/amt-2022-81.

———. 2022b. "Combining Mie–Raman and Fluorescence Observations: A Step Forward in Aerosol Classification with Lidar Technology." *Atmospheric Measurement Techniques* 15 (16): 4881–4900. https://doi.org/10.5194/amt-15-4881-2022.

Veselovskii, Igor, Qiaoyun Hu, Philippe Goloub, Thierry Podvin, Marie Choël, Nicolas Visez, and Mikhail Korenskiy. 2021. "Mie–Raman–Fluorescence Lidar Observations of Aerosols during Pollen Season in the North of France." *Atmospheric Measurement Techniques* 14 (7): 4773–86. https://doi.org/10.5194/amt-14-4773-2021.

Veselovskii, Igor, Qiaoyun Hu, Philippe Goloub, Thierry Podvin, Mikhail Korenskiy, Olivier Pujol, Oleg Dubovik, and Anton Lopatin. 2020. "Combined Use of Mie–Raman and Fluorescence Lidar Observations for Improving Aerosol Characterization: Feasibility Experiment." *Atmospheric Measurement Techniques* 13 (12): 6691–6701. https://doi.org/10.5194/amt-13-6691-2020.

Zieger, P., Aalto, P. P., Aaltonen, V., Äijälä, M., Backman, J., Hong, J., Komppula, M., Krejci, R., Laborde, M., Lampilahti, J., de Leeuw, G., Pfüller, A., Rosati, B., Tesche, M., Tunved, P., Väänänen, R., and Petäjä, T.: Low hygroscopic scattering enhancement of boreal aerosol and the implications for a columnar optical closure study, Atmos. Chem. Phys., 15, 7247–7267, https://doi.org/10.5194/acp-15-7247-2015, 2015

https://www.icare.univ-lille.fr/dev/jdescloitres/gallery/public/gallery_2021_02_saharan_dust/

https://www.bipm.org/en/publications/si-brochure